CrystEngComm

Accepted Manuscript

ROYAL SOCIETY OF CHEMISTRY

www.rsc.org/crystengcomm

Effect of High Pressure on the Crystal Structure and Charge Transport Properties of (2-fluoro-3-pyridyl)(4-iodophenyl)borinic 8-oxyquinolinate complex

Grzegorz Wesela-Bauman,[a,b]* Simon Parsons,[c] Janusz Serwatowski,[a] Krzysztof Woźniak[b]

[a]*Physical Chemistry Department, Faculty of Chemistry, Warsaw University of Technology, Noakowskiego 3, 00-664 Warszawa, Poland*
[b]*Department of Chemistry, University of Warsaw, Pasteura 1, 02-093 Warszawa, Poland.*
[c]*School of Chemistry and Centre for Science at Extreme Conditions, The University of Edinburgh, King's Buildings, West Mains Road, Edinburgh EH9 3JJ, Scotland.*

*Corresponding authors: grzegorz.wesela@chem.uw.edu.pl

KEYWORDS

high pressure, borinic derivatives, X-ray structure, charge transporting materials, luminescent materials

ABSTRACT

The crystal and molecular structure of (2-fluoro-3-pyridyl)(4-iodophenyl)borinic 8-oxyquinolinate has been determined at room temperature at pressures ranging from ambient to 4.9 GPa in approximately 1 GPa steps. The crystal structure symmetry is conserved during the compression while the *a*, *b* and *c* unit-cell dimensions were compressed by 7.5%, 8.0% and 6.9%, respectively. The crystal cell volume decreased by 19.4%. The analysis of the compression of the crystal was supported by computational results obtained with *PASCAL* code. They proved that the crystal compression proceed almost isotropically. A combination of Hirshfeld surface analysis and *PIXEL* calculations indicated the formation of multiple new contacts involving Fluorine...Fluorine and Iodine...π-density. Energies of interactions calculated for the observed motifs present in the crystal were rationalized on the basis of contacts observed for these motifs. Further analysis based on the Marcus model was performed to trace the possible changes in the charge transport properties of the crystal. The analysis showed that electron and hole transport properties are not affected in the same way by the compression. However, hydrostatic pressure did not affect which charge transport (electron or hole) is the dominating one for this material.

INTRODUCTION

8-oxyquinlinate complexes, MQ_n(n=1,2,3) (M is trivalent metal and Q is 8-oxyquinolinate), are widely used in organic light emitting diodes (OLEDs) as light emitters and charge carriers.[1] Though materials with M = Al were frequently used both as emitting materials[2] and as charge transport carriers,[3] their good optical properties were counterbalanced by long term instability leading to degradation of the diode.[4,5] Hence, analogues of aluminium were investigated, mainly GaQ_3 and InQ_3 complexes.[6–8] Finally, borinic complexes turned out to be more stable and more efficient emitters than aluminium[9,10] and became widely investigated.[11–15] For MQ_n(n=1,2,3) complexes, it is commonly believed that the HOMOs span across the phenolate ring and the LUMOs across the pyridine ring of the 8-oxyquinolinate. Those orbitals are involved in processes of electron excitation and relaxation followed by photon emission. The energies of the frontier orbitals can be affected by, either, chemical functionalisation (by attaching electron donating or withdrawing groups)[16–18] or by modification of their crystal structure which was proven by high pressure studies on structures of AlQ_3, GaQ_3 and InQ_3.[19]

Important parameter of a particular material, from the standpoint of application in OLEDs, is the charge transfer character and its rate.[20,21] In this matter, it is interesting that some authors were able to point the correlation between the degree of intermolecular π-π interactions and charge transport properties and electroluminescence.[22,23] However, in those papers authors were simultaneously changing the molecular and, as a consequence, supramolecular structure. Studies of influence of the crystal phase, without affecting the molecular structure, were done with AlQ_3.[24] Broader description of the impact of molecular arrangements were done with computational studies.[25–33] This approach assumes that carrier mobility (μ) in the hopping process is related to charge transfer rate (k_{CT}) *via* the Einstein equation (1):

$$\mu = \frac{ed^2}{k_B T} k_{CT} \quad (1)$$

where k_B is the Boltzmann constant, T is temperature, e the electronic charge, and d is the transport distance. The charge transport rate can be calculated using Marcus-Hush theory.[34–36] The charge transport (CT) rate constant, k_{CT}, can be evaluated by the following equation (2):

$$k_{CT} = \frac{2\pi}{\hbar} H_{AB}^2 \frac{1}{\sqrt{4\pi \Lambda k_B T}} \exp\left(-\frac{(\Delta G^o - \Lambda)^2}{4\Lambda k_B T}\right) \quad (2)$$

where Λ is reorganization energy, H^2_{AB} is the transfer integral which represents the electronic coupling between donor and acceptor, T is the temperature, ΔG^o is the standard free enthalpy and k_B is the Boltzmann constant. Since analysis of hopping of charge carriers between molecules of the same compound than the standard free enthalpy is equal zero ($\Delta G^o = 0$). Furthermore the reorganization energy (Λ) is a constant value for a particular compound. The only parameter affected by interactions in the crystal state is the transfer integral (H_{AB}). The greater values of the transfer integral for a particular type of the charge carriers (for a single contact) the better pathway for charge hopping such contact is ($\mu \sim H_{AB}$). This integral is related to the energetic splitting (ΔE) of the electronic level of two interacting molecules (**Figure 1**).

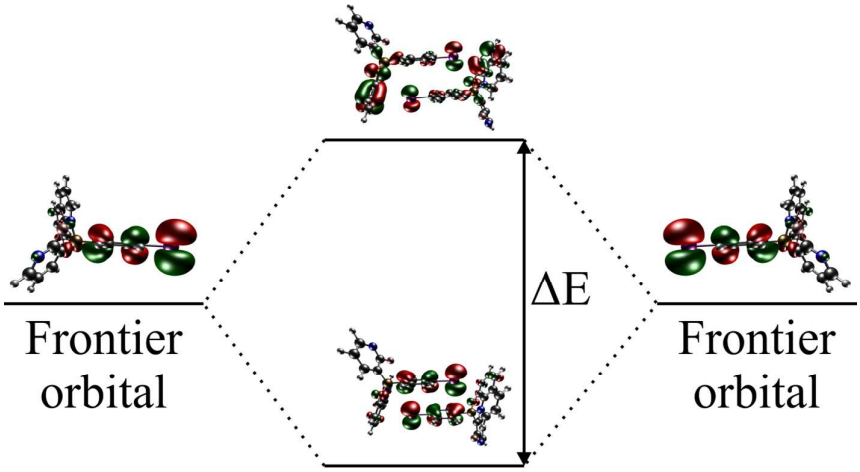

Figure 1. Energetic splitting of the frontier orbitals.

H_{AB} for hole and electron transport is equal the half of the energy difference between HOMO and HOMO−1 or LUMO and LUMO+1 energy levels, respectively.

Recently, we have investigated the influence of functionalization on the photophysical properties of (2-fluoro-3-pyridyl)aryloborinic 8-oxyquinolinates.[37] In this paper, we extend these investigations by determining the effect of pressure on the crystal structure of (2-fluoro-3-pyridyl)(4-iodophenyl)borinic 8-oxyquinolinate (**1**, **Figure 2**) and its charge transfer properties.

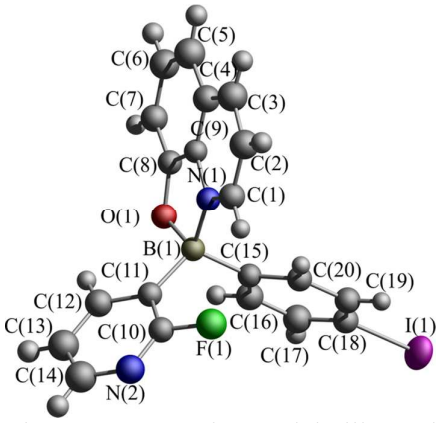

Figure 2. Molecular structure and atom labelling scheme for the complex **1.**

In this contribution, the crystal structure of **1** at pressure ranging from ambient to 4.9 GPa is presented. The impact of high pressure on weak interactions is described and discussed. Experimental results are supported by theoretical analysis of the influence of the pressure on the charge carrier properties in the framework of the Marcus theory.

EXPERIMENTAL SECTION

Synthesis, crystal growth and high-pressure crystallography. The title compound was synthesized according to our previous report.[37] Crystals of **1** were grown by a slow evaporation of acetone from a concentrated solution of **1**. One block-shaped crystal of dimensions 0.2 x 0.2 x 0.25 mm was selected and loaded into a Merrill–Bassett diamond–anvil cell (DAC).[38,39] The cell total opening angle is 80°, and the cell was equipped with 600 μm culets and a tungsten gasket. A 4:1 mixture of methanol and ethanol was used as a hydrostatic medium. A small piece of ruby was also put into the cell as the pressure marker with the ruby fluorescence method used to measure the pressure.[40]

Data collection, reduction and refinement. Single-crystal X-ray data collection was conducted at ambient pressure and at 0.17, 1.09, 2.04, 3.02, 3.96 and 4.88 GPa. All high-pressure data were collected at ambient temperature. Diffraction data were collected on a Bruker APEX II diffractometer with a graphite-monochromated MoK_α radiation, λ = 0.71073 Å.[41] The data were integrated using *SAINT*[42] and an absorption correction was performed with the *SADABS* program.[43] Dynamic masking was applied during integration of the high-pressure data sets.[44]

The structure under ambient conditions was solved using the *SUPERFLIP*[45] program implemented in *CRYSTALS*.[46] The independent atom model (IAM) refinement based on *F* was performed with the *CRYSTALS* package. Optimised weighting schemes based on Chebychev polynomials were used for all refinements.[47] Atomic scattering factors in their analytical form

were taken from the International *Tables for Crystallography*.[48] All non-hydrogen atoms (except iodine) were refined isotropically and all of the hydrogen atoms were placed in idealized positions within the riding model for Atomic Displacement Parameters (ADPs) (with $U_{iso}^{H} = 1.2 \cdot U_{eq}^{C}$) in order to retain a data-to-parameter ratio greater than 24. All hydrogen atoms were clearly visible on the difference density maps. Coordinates (and ADPs) of **1** were refined against these ambient pressure X-ray data to yield a conventional R_1 factor of 5.1% for 2650 data with $I > 2\sigma(I)$.

Every data set was restricted to 0.84 $Å^{-1}$ resolution in order to have a meaningful comparison of the geometries obtained from the experiments. For every collected data set the $F_o^2 > 2\sigma(F_o^2)$ criterion, adopted form *Shelx*, was used only for calculating *R* factors and is not relevant to the choice of reflections for the refinement.

Starting models for the high-pressure structures were as taken from the coordinates determined in the previous step. Minimization was performed against *F* using data with $I > 2\sigma(I)$. The completeness of the data-sets was ranging from 37% to 46%, and only the iodine was refined with anisotropic displacement parameters, all other atoms being modelled isotropically. It is worth to mention that the data quality for all the pressure steps was sufficient enough to perform anisotropic refinement of the ADPs for all the atoms (not just for the iodine atom).

All hydrogen atoms were clearly visible on the difference density maps. Hydrogen atoms were placed in idealized positions and allowed to ride on their parent atoms with $U_{iso}^{H} = 1.2 \cdot U_{eq}^{C}$. All bond distances and angles were restrained to values observed in the ambient pressure structure. Details of data collection and refinement are provided in **Table 1** and, with more details, in the Supporting Information (**Table S1**).

CCDC 993575-993581 contains the supplementary crystallographic data (CIF files) for crystals studied in this work. They can be obtained free of charge from the Cambridge Crystallographic Data Centre *via* www.ccdc.cam.ac.uk/data_request/cif or from the authors.

Theoretical calculations and visualization. Energies of intermolecular interactions were calculated using the *PIXEL* method.[49–52] For comparison of results obtained with *PIXEL* and DFT and post-HF methods see reference [[53]]. All quantum calculations were carried out using the *GAUSSIAN09* package.[54] Calculation of the frontier orbitals energies employed the B3LYP[55,56] and B97D[57] DFT potentials combined with 6-31+g(d,p)[58] basis set. The LANL2DZ[59] basis set with its complete-core relativistic effective core potential was used for iodine atom. Additional *d*- and *f*- functions were added to the LANL2DZ basis set according

to the modification proposed by Glukhovtsev *et al*.[60] Benchmark calculations demonstrated that this modification improves obtained bond lengths and bond energies leading to a more accurate results.[61,62] Our previous work implementing this modification showed good correlation between experimental and theoretically obtained UV-Vis spectra.[37] Electron density was evaluated with DGDZVP[63,64] basis set. C-H distances were normalized prior to calculations to the standard neutron values 1.083Å.[65] Visualization of the crystal structures and frontier orbitals were achieved using the *DIAMOND*[66] and the *VMD*[67] programs, respectively. The electrostatic potential was calculated and visualized with *AIMALL*.[68] Hirshfeld surface analysis was performed with *CRYSTALEXPLORER*.[69–72]

Table 1. Selected crystallographic data for compound **1**.

Experimental details	**(1) T= 296 K ambient**	**(2) T= 296 K P = 0.17 GPa**	**(3) T= 296 K P = 1.09 GPa**	**(4) T= 296 K P = 2.04 GPa**	**(5) T = 296 K P = 3.02 GPa**	**(6) T= 296 K P =3.96 GPa**	**(7) T= 296 K P = 4.88 GPa**
Chemical formula	$C_{20}H_{13}BFIN_2O$	$C_{20}H_{13}BFIN_2O$	$C_{20}H_{13}BFIN_2O$	$C_{20}H_{13}BFIN_2O$	$C_{20}H_{13}BFIN_2O$	$C_{20}H_{13}BFIN_2O$	$C_{20}H_{13}BFIN_2O$
M_r	454.03	454.03	454.03	454.03	454.03	454.03	454.03
Crystal system space group	Monoclinic $P2_1/n$	Monoclinic $P2_1/n$	Monoclinic $P2_1/n$	Monoclinic $P2_1/n$	Monoclinic $P2_1/n$	Monoclinic $P2_1/n$	Monoclinic $P2_1/n$
Cell settings: a,b,c (Å)	6.8581(2) 14.7849(4) 17.3015(6)	6.8234(4) 14.7074(7) 17.200(2)	6.6545(2) 14.3261(5) 16.7183(14)	6.5502(4) 14.1051(7) 16.497(3)	6.4636(2) 13.8775(5) 16.3094(16)	6.4012(4) 13.7152(9) 16.187(3)	6.3469(5) 13.6039(10) 16.105(3)
α,β,γ (°)	90.000 90.966(2) 90.000	90.000 90.814(7) 90.000	90.000 90.460(5) 90.000	90.000 90.396(8) 90.000	90.000 90.317(5) 90.000	90.000 90.438(8) 90.000	90.000 90.549(10) 90.000
V (Å^3)	1754.06(9)	1725.9(2)	1593.75(15)	1524.1(3)	1462.91(16)	1421.1(3)	1390.5(3)
Z	4	4	4	4	4	4	4
d (Mg·m^{-3})	1.719	1.747	1.892	1.979	2.061	2.122	2.169
Crystal form, colour	block, green	block, green	block, green	block, green	block , green	block , green	block , green
Crystal size (mm)	0.20x0.20x0.25	0.20x0.20x0.25	0.20x0.20x0.25	0.20x0.20x0.25	0.20x0.20x0.25	0.20x0.20x0.25	0.20x0.20x0.25
No. of measured, independent and observed [$F^2>2\sigma(F^2)$]	34795 5362 2650	9268 1184 936	8787 1141 887	7648 1067 871	8296 4171 949	6840 1142 916	6772 1187 910
Criterion for observed reflection	$I > 2.00\sigma(I)$	$I > 2.00\sigma(I)$	$I > 2.00\sigma(I)$	$I > 2.00\sigma(I)$	$I > 2.00\sigma(I)$	$I > 2.00\sigma(I)$	$I > 2.00\sigma(I)$
Completeness (%)	100	37	39	38	42	44	46
R_{int} (%)	6.5	5.6	4.3	4.0	4.3	4.4	5.7
Θ_{max}	30.53	25.38	25.38	25.38	25.33	25.35	25.54
Refinement on	F	F	F	F	F	F	F
R[$F^2>2\sigma(F^2)$],	0.0510	0.0501	0.0354	0.0326	0.0339	0.0340	0.0392
wR(F^2),	0.0512	0.0396	0.0385	0.0348	0.0355	0.0367	0.0417
GooF	1.000	1.000	1.000	1.000	1.000	1.000	1.000
No. of reflections	2650	936	887	871	949	916	910
No. of parameters	110	110	110	110	110	110	110
$\Delta\rho_{max}$, $\Delta\rho_{min}$ (eÅ^{-3})	0.70, −0.78	0.40, −0.40	0.58, −0.43	0.37, −0.30	0.46, −0.33	0.34, −0.50	0.52, −0.66

RESULTS AND DISCUSSION

Molecular shape. The tetrahedral character of the coordination sphere of the boron atom is not affected by pressure. The bond lengths of the dative bonds: B-N, and B-O, and B-C are equal within error at all pressures studied (**Table S2**). Similarly, there are no significant differences in the molecular dimensions involving phenyl and pyridyl groups. High pressure slightly modifies the conformation of the molecule. The most pronounced differences between the ambient and 4.9 GPa geometry of the moiety can be summarized as a twist of quinoline rings and deviation from planarity in the pyridine ring with interplane angles equal 3.6º and 5.7º, respectively (**Figure S6**). Hence, as expected for this material, the only thing that was affected by the pressure were the intermolecular interactions which can be directly related to the change in the CT properties.

The structure of 1 at ambient temperature and pressure. The supramolecular architecture of **1** is based on crystallographic motifs compromising weak interactions (**Figure 3** and **5**). The strongest motif [see (1)] involves bifurcated hydrogen bond C(1)-H(1)…N(2) ($d_{H...N}$ = 2.63 Å) and C(2)-H(2)…N(2) ($d_{H...N}$ = 2.88 Å). The energy of this motif is equal to −53.1 kJ mol^{-1} and a significant electrostatic (**Figure 3**, **Table 2**) character. The impact of F(1)…F(1) interaction on the stability of this motif is not clear as the halogen-halogen distance is equal to $d_{F...F}$ = 3.197(4) Å, which is relatively close to the sum of the van der Waals-radii (2.94 Å).[73]

The second most energetic (2) motif comprises a bifurcated hydrogen bond: C(19)-H(19)…O(1) ($d_{H...O}$ = 2.54 Å) and C(20)-H(20)…O(1) ($d_{H...O}$ = 2.76 Å), with the energy of interactions equal to −40.7 kJ mol^{-1}. This is a dispersion-dominated motif which features interaction between 8-quinolinates. Repulsion, on the other hand, cannot be as easy rationalized by structural interactions as the mutual proximity of hydrogen-fluorine atoms, mainly C(12)-H(12)…F(1) and C(13)-H(13)…F(1) interactions (with interatomic distances equal to 2.67 Å and 2.81 Å, respectively) has larger distances than the ones observed in similar structures (2.43-2.73 Å).[37] For this motif we observed a mutual proximity of H(16) and H(19) atoms but the distance between those hydrogens ($d_{H...H}$ = 2.23 Å) is much greater than approximate limit (1.7 Å) for such contacts established by Wood *et al*.[74]

The energy of interaction (3) in this case is dominated by a repulsive interactions (101.5 kJ mol^{-1}), which is balanced by electrostatic (−48.8 kJ mol^{-1}) and dispersion terms (−67.1 kJ mol^{-1}). Those stabilizing contributions to the energy of (3) can be rationalized by existence of a short intermolecular contact between C(9) and I(1) measuring 3.591(4) Å, and

the interplanar contact between the 4-iodophenyl moieties with interplane distance equal 4.024 Å.

Table 2. The comparison of the energies of interactions in crystal structure of **1** at ambient pressure and at 4.9 GPa (*italic*). Calculated using *PIXEL*.

		Energy (kJ mol^{-1})					
	d (Å) [1)]	Electrostatic	Polarization	Dispersion	Repulsion	Total	Symmetry
(1)	8.074	−42.7	−13.7	−24.9	28.2	−53.1	1−x, 1−y, 1−z
	7.662	*−85.6*	*−29.6*	*−40.9*	*106.5*	*−49.6*	*1−x, 2−y, 1−z*
(2)	6.858	−26.2	−11.1	−44.5	41.0	−40.7	x±1, y, z
	6.347	*−107.4*	*−45.6*	*−90.8*	*201.1*	*−42.8*	*x±1, y, z*
(3)	8.998	−48.8	−20.6	−67.1	101.5	−35.0	1−x, −y, 1−z
	8.406	*−193.0*	*−73.2*	*−128.7*	*363.0*	*−31.2*	*1−x, 1−y, 1−z*
(4)	9.267	−26.4	−10.2	−38.3	42.4	−32.6	x±0.5, 0.5−y, z±0.5
	8.638	*−98.6*	*−46.4*	*−80.9*	*197.5*	*−28.3*	*x±0.5, 1.5−y, z±0.5*
(5)	8.485	−18.1	−6.7	−25.4	21.8	−28.4	−x, −y, 1−z
	7.755	*−49.0*	*−26.1*	*−49.9*	*87.6*	*−37.3*	*−x, 1−y, 1−z*
(6)	7.498	−18.9	−10.9	−47.7	50.9	−26.6	−x, 1−y, 1−z
	6.942	*−95.8*	*−52.9*	*−94.2*	*224.8*	*−18.1*	*−x, 2−y, 1−z*
(7)	9.374	−1.9	−3.1	−13.8	5.4	−13.3	x±0.5, 0.5−y, z±0.5
	8.695	*−21.2*	*−18.7*	*−37.1*	*53.6*	*−23.4*	*x±0.5, 1.5−y, z±0.5*
(8)	12.336	−7.7	−2.7	−11.2	12.4	−9.2	0.5−x, y±0.5, 1.5−z
	11.738	*−25.4*	*−9.5*	*−21.7*	*45.7*	*−10.9*	*0.5−x, y±0.5, 1.5−z*
(9)	10.516	−2.7	−0.5	−1.9	0.0	−5.0	0.5−x, y±0.5, 0.5−z
	9.498	*−4.5*	*−0.8*	*−3.7*	*0.1*	*−8.8*	*0.5−x, y±0.5, 0.5−z*
(10)	12.970	−3.3	−0.1	−0.3	0.0	−3.6	2−x, 1−y, 1−z
	12.718	*−2.8*	*−0.5*	*−4.5*	*0.6*	*−7.2*	*2−x, 1−y, 1−z*

[1)] *d* parameter designates the distance between the centre of masses of two interacting molecules.

The charge distribution of halogen moieties is not isotropic (**Figure 4**), and the short distance is indicative of an interaction involving the σ-hole of the iodine and the π-electrons of the 8-oxyquinlinate rings. Although, the repulsion between the π-electrons of 4-iodophenyl moieties and negatively charged part of the iodine atom may be counterbalancing attractive force between σ-hole and 8-oxyquinolinate rings.

The fourth motif (4) builds chains of molecules disposed about the 2_1 screw axis. Stabilization of this motif results from joint effects of dispersion (−38.3 kJ mol^{-1}) and the electrostatic interactions (−26.4 kJ mol^{-1}). This is achieved with significant contribution of the C-H… π type interactions, mainly, C(6)-H(6)…Cg(1) ($d_{H...Cg}$ = 2.88 Å, C(6)-H(6)-Cg(1) = 152), where Cg(1) is the centroid calculated for the 2-fluoro-3-pyridyl moiety. The largest

contribution to the energy of interactions for this motif, according to the *PIXEL* calculations, is, like in the third motif, dominated by the repulsion term (42.4 kJ mol^{-1}).

The fifth motif (5) is also based on the anisotropy of charge distribution of the iodine atom. It is stabilized by C(7)-H(7)…I(1) interactions in which positively charged proton is pointing towards negatively charged side of the iodine atom.

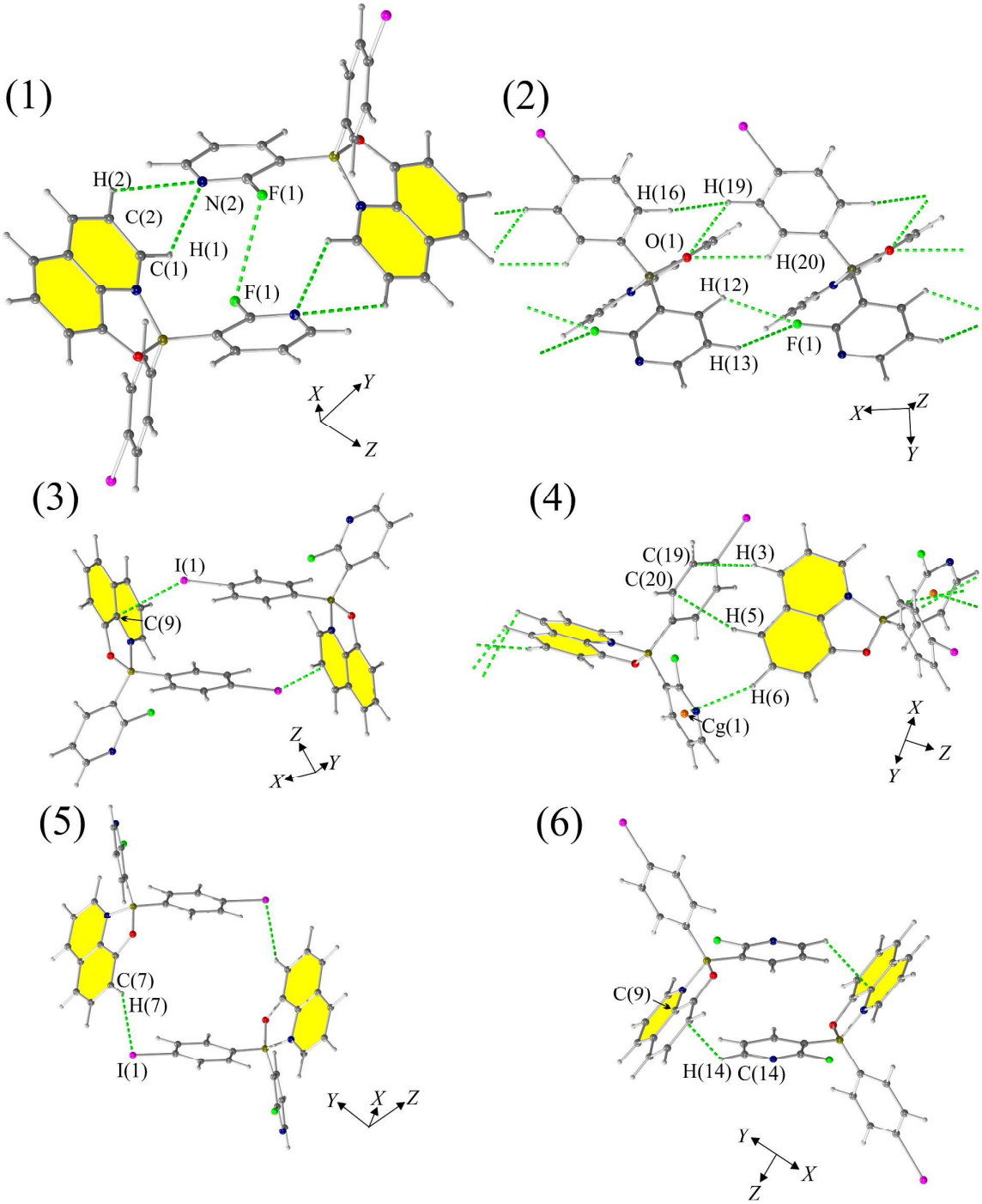

Figure 3. Motifs (1)-(6) observed in the crystal structure of **1**.

The sixth (6) motif is based upon two sets of interactions. The first set of interactions is based on C-H...π interactions, with the distance between C(9) and H(14) atoms from 2-fluoro-3-pyridyl moiety equal to 2.86 Å. The other set of interactions is constructed from the π...π stacking interactions between 2-fluoro-3-pyridyl moieties with the interplanar distance equal to 3.780 Å. We believe that this interaction is strong as, according to the calculations done by Sherill *et al*,[75] such distance is quite favourable for π…π interactions.

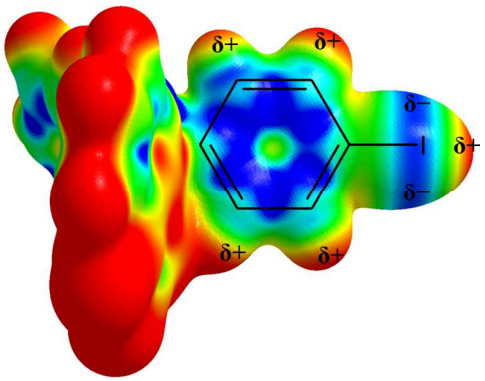

Figure 4. The anisotropic charge distribution around the iodine atom in **1**. Electrostatic potential calculated at B3LYP/DGDZVP level of theory.

Motifs (7)-(10) (**Figure 5**) compromise very weak interactions and are stabilized by either dispersion (motifs 7 and 8) and/or electrostatic contributions (motifs 8, 9 and 10). The seventh motif (7) has a short H(3)…H(16) contacts (2.58 Å) and molecules in this motif are arranged in such a way so they create a chain of molecules. Similar chains are created by motifs (8) and (9) and stabilized by Q…Q interactions. Motif (10) compromise interacting molecules for which mutual distance permits only electrostatic interactions.

Impact of pressure on the crystal structure of compound 1.

Effect of the pressure on the unit cell dimensions. Compound **1** is stable up to at least 4.9 GPa. The *a*, *b* and *c* unit-cell dimensions decrease by 7.5% 8.0% and 6.9%, respectively. The *β* angle decreases by 0.4°. The volume of **1** is reduced by 19.4%. The lattice parameters as a function of pressure have been shown in **Figure S1** and **Figure S2**. The degree of lattice distortion (DLD), calculated by program *STRAIN*,[76–78] is equal to 0.0415 (for output of the *STRAIN* program and see Supporting Information). For comparisment, similar values of DLD parameter can be obtained for ruthenium complexes at 4.63 GPa (0.0419),[79]and much lower values of DLD are observed for L-alanine at 4.31 GPa (0.0337).[80]

The changes of the variable-pressure parameters of the unit cell for this low symmetry system are not strictly related to the compressibility, which was presented by Cliffe *et al*.[81] Hence we have implemented the *PASCAL* code for these calculations (for output of the

PASCAL program see Supporting Information).[81] Since the β angle is close to 90°, the *PASCAL* analysis gave similar results as the analysis for nonorthogonal *a*, *b* and *c* cell parameters. Direction of the greatest strain is close to the X axis (see orthonormalization matrix in Supporting Information) and can be rationalized as a consequence of lack of interactions parallel to that direction.

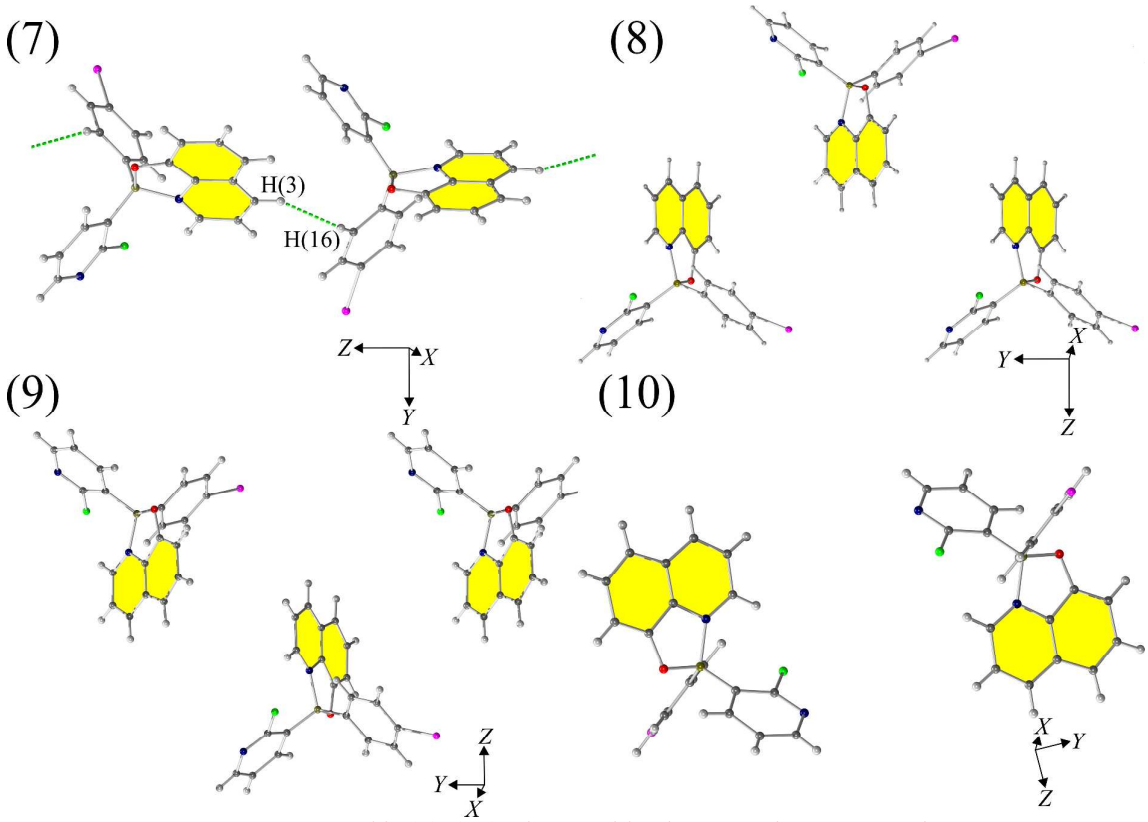

Figure 5. Motifs (7)-(10) observed in the crystal structure of **1**.

Analysis based on Birch-Murnaghan coefficients (B and B') may indicate a rapid stiffening of the described material (B' > 4) with pressure (for more details and comparisment with other materials see Supporting Information).

Effect of the pressure on contacts lengths and energies. Impact of the pressure on the intermolecular contacts was evaluated thorough *PIXEL* calculations and depicted in **Figure 6** (**Figure S9**, **Table S4-S10**). Increase of hydrostatic pressure results in shortening of intermolecular distances for all motifs. For Motif (7) it seems that change of pressure form 3.96 to 4.88 GPa didn't affect *d* parameter significantly. After initial compression the distances of interactions for all motifs were lowered but at higher pressures the effect of pressure was different depending on the nature of contacts present in the structure. The

energies of motifs (2), (3), (5) and (7) during compression passed through global energy minimum and then raised. On the other hand motif (4) passed through global maximum and then reach a local minimum at 4.9 GPa. The weakest motifs (*e.g.* (8), (9) and (10)) were becoming more stable at each pressure step.

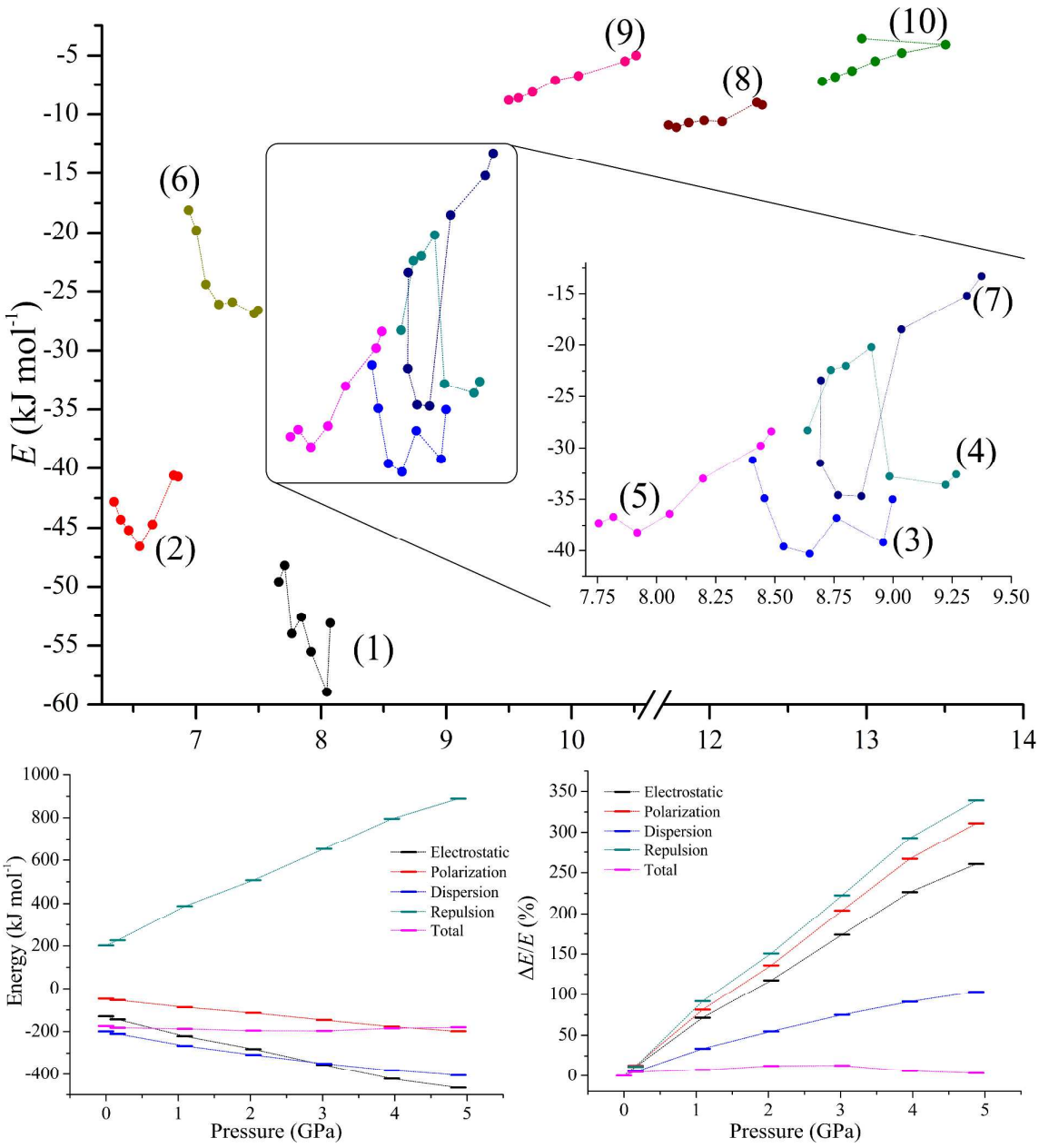

Figure 6. Energies of motifs (1)-(10) as a function of distance (upper graph) and lattice energy (together with contributions from electrostatic, polarization, dispersion and repulsion) as a function of pressure (lower graphs). Calculated using *PIXEL*.

The effect of high pressure on the intermolecular interaction can be visualised using Hirshfeld (d_{norm}) surface analysis (**Figure S2-S4**). Red areas on surface which represents contacts which existed at ambient pressure become more pronounced after compression. New contacts appeared, especially H…H and C…H, but also F…F and N…H type contacts. Interactions between the iodine atom with both phenyl and Q rings become prominent at elevated pressure.

Compression has affected both lattice energies and contributions to the lattice energies (**Figure 6**, lower graphs). As the compression progresses the total lattice energies decreases to reach minimum at *ca* 2.5 GPa and then their values start to increase. It seems that such behaviour is a consequence of interplay between the polarization and the repulsion terms which are becoming more prominent with pressure (more than 3x times stronger than at ambient pressure, **Table S2-S3**).

Estimated change in the CT properties of 1 with pressure. Motifs described earlier were analyzed in terms of their charge transport properties using Marcus theory. An interesting phenomenon is that a slight squeeze of the crystal improved electron transporting properties (understood as an increase of $H_{AB}(e^-)$) of the crystal and decrease the hole transporting properties (understood as a decrease of $H_{AB}(h^+)$) (**Figure 7**). This is something that made the properties of the crystal more pronounced. It may be also point to the fact that the pattern of interactions at this pressure is suppressing the hole transport. Further increase of the hydrostatic pressure resulted in a simultaneous increase of the $H_{AB}(e^-)$ and $H_{AB}(h^+)$, the former one seem to be more affected by pressure.

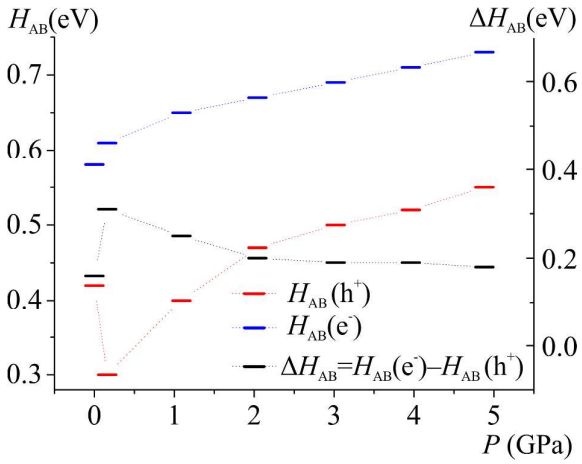

Figure 7. Sum of charge transfer integrals as a function of hydrostatic pressure calculated at B97D/6-31+g(d,p) level of theory.

It seems that crystallographic motifs are not participating in the CT properties equally, nor their character is not fixed during compression (**Figure 8a** and **8b**). The biggest contributions to the CT are form motifs (3), (4) and (7). Motifs (3) with Iodine…π-density interaction is almost solely a hole transporting contact, which CT properties are being increased with compression. It seems that this motif is being destabilized by the pressure. On the other hand, motifs (4) and (7) have both dominating electron transporting properties. They also present the same pattern of CH…π interactions between **Q** and 2-fluoro-3-pyridyle and 4-iodophenyl rings. It seems as mutual proximity between electron-rich phenolate ring and electron-deficient 2-fluoro-3-pyridyl ring favours transport of electrons. As the compression proceeds for (4) the electron CT properties are being hampered by increasing interactions between two electron-deficient rings, mainly pyridine and 2-fluoro-3-pyridyl. At 4.9 GPa mutual orientation of molecules is similar to the one observed for the normal pressure. Therefore, reinforcement of electron CT properties is being observed. Similar situation is being observed for motif (7). For pressure steps with close proximity of phenolate ring and 2-fluoro-pyridyl the electron transporting properties were reinforce. Whereas for the ones which favours pyridine and 2-fluoro-pyridyl the CT properties were hampered. Observed trends in CT properties seems to be corelated with the stablization energies (**Figure 6**). For those two motifs the stronger they are the better CT properties they are presenting.

At this point it should be stressed that the *PIXEL* method was checked against various methods (DFT, post-HF).[53] The corelation was established against stablization energies dervied with *PIXEL* and *ab initio* methods leading to a conslucion that the method work fine. However, in this contribution we are seeing that orbital overlaping (important from the standpoint of charge hoping) obtained with *ab initio* methods in some cases is corelating with motif energies obtained with *PIXEL*.

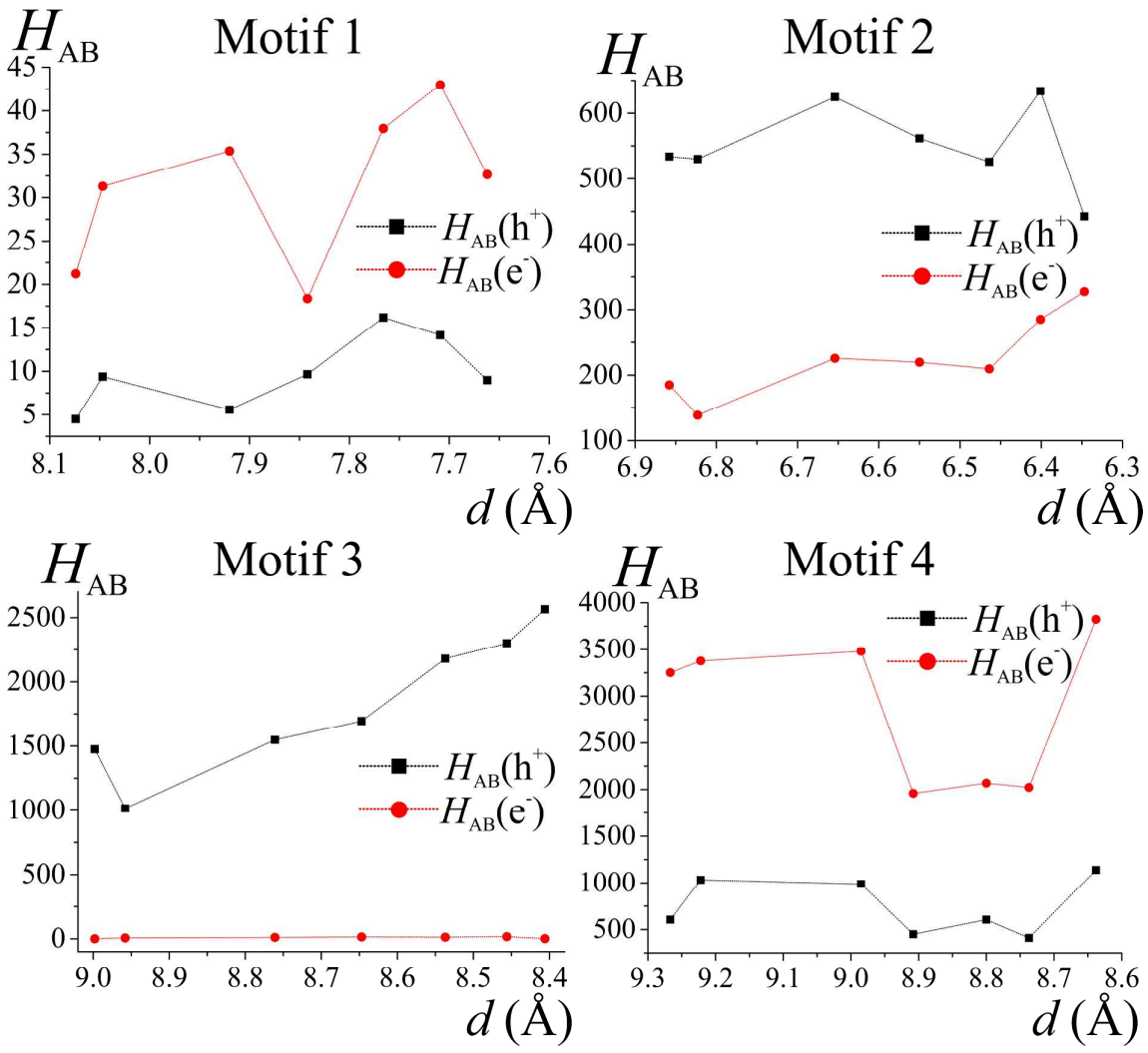

Figure 8a. Charge transfer integrals ($H_{AB}(10^{-4}$ eV)) for motifs (1)-(4) as a function of hydrostatic pressure calculated at B97D/6-31+g(d,p) level of theory.

Apart for (3) also motifs (2) and (5) have their hole transporting properties dominating over electrons. This is due to the proximity of 4-iodophenyl rings which are being occupied by HOMO orbitals. The CT character of motifs (8) and (9) was changed by the compression. It seems that mutual orientation of molecules in those two motifs promotes a better charge hopping that the one present in motif (1).

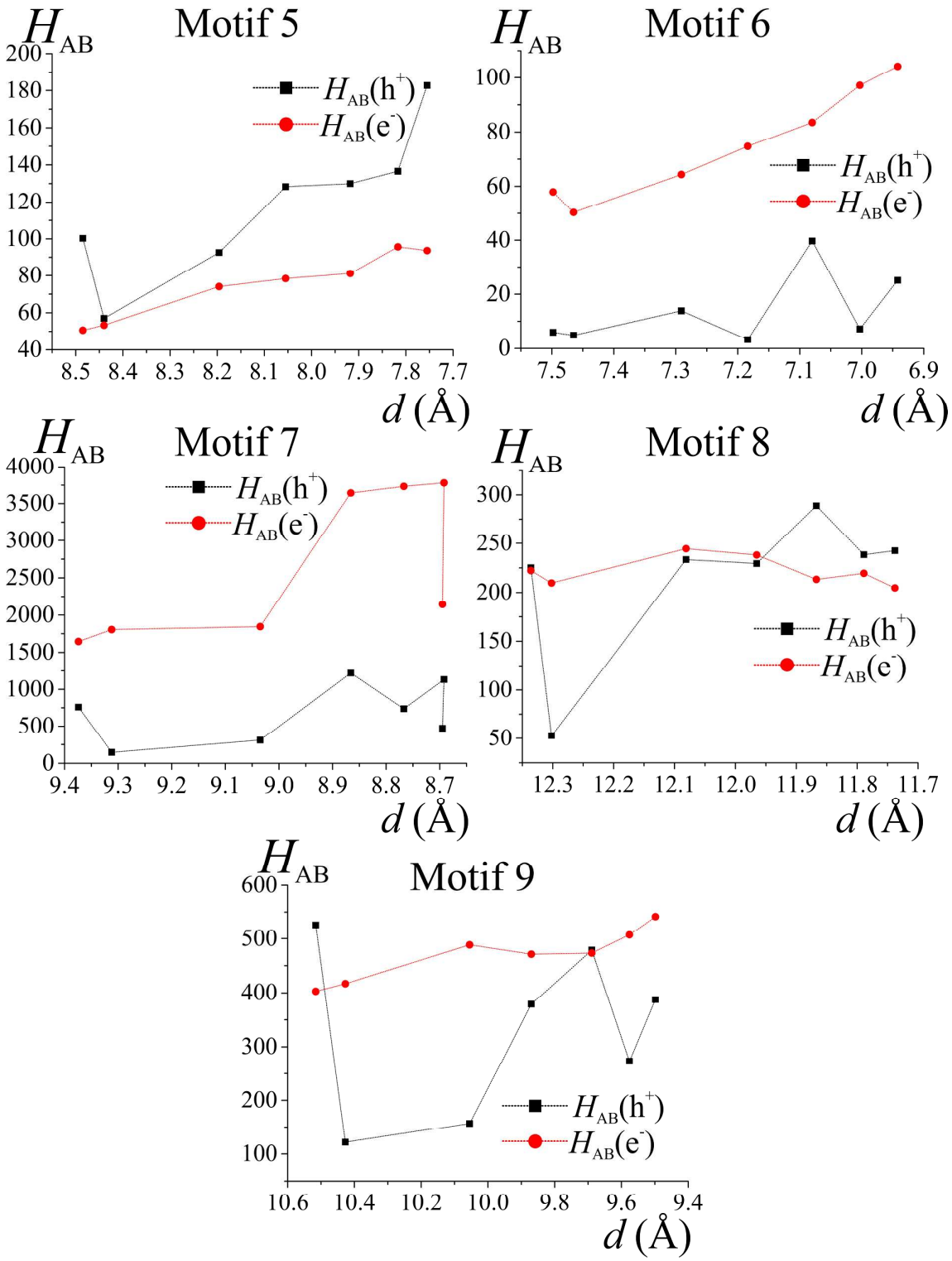

Figure 8b. Charge transfer integrals ($H_{AB}(10^{-4}$ eV)) for motifs (5)-(9) as a function of hydrostatic pressure calculated at B97D/6-31+g(d,p) level of theory.

CONCLUSIONS

Crystal of **1** was compressed almost isotropically which was confirmed by the analysis of the crystal lattice parameters supporting the analysis in *PASCAL* and *STRAIN* programs. While the molecular geometry remains virtually unchanged, the intermolecular interactions were affected greatly by the pressure. This was pointed qualitatively by Hirshfeld surface analysis and quantitivaly by *PIXEL* calculations. Having a detailed description of a crystal system and changes triggered by the pressure we could estimate how the structure affects the charge transport properties. It turns out that an increase of pressure improved charge transport properties estimated with the Marcus theory. It seems that motifs based on interactions between electron-rich and electron-poor ligands have strong electron transporting properties. On the other hand interactions between two electron-deficient counterparts may hamper electron transporting properties.

ACKNOWLEDGEMENTS

The MPD/2010/4 project is realized within the MPD programme of Foundation for Polish Science, cofinanced from European Union, Regional Development Fund. This work was supported by the Warsaw University of Technology and by the Polish Ministry of Science and Higher Education (Grant No. DEC-2011/03/B/ST5/02755). The support by Aldrich Chemical Co., Milwaukee, WI, U.S.A., through continuous donation of chemicals and equipment is gratefully acknowledged. G.W.B. thanks the Foundation for Polish Science for financial support within the **International PhD Program**. Authors gratefully acknowledge The Interdisciplinary Centre of Mathematical and Computational Modelling in Warsaw (grant no. G33-14) for providing computer facilities on which most of the calculations were done. G.W.B. would like to thank Dr Stephen Moggach, Mr Andrew Maloney and Mr Chris Cameron from Chemical Crystallography Research Group at The University of Edinburgh.

REFERENCES

1. C. H. Chen and J. Shi, *Coord. Chem. Rev.*, 1998, **171**, 161 – 174.
2. S. A. VanSlyke and C. W. Tang, *Appl Phys Lett*, 1987, **51**, 913–915.
3. B. C. Lin, C. P. Cheng, Z.-Q. You, and C.-P. Hsu, *J. Am. Chem. Soc.*, 2005, **127**, 66–67.
4. Z. D. Popovic, H. Aziz, A. Ioannidis, N.-X. Hu, and P. N. M. dos Anjos, *Synth. Met.*, 2001, **123**, 179 – 181.
5. J. E. Knox, M. D. Halls, H. P. Hratchian, and H. Bernhard Schlegel, *Phys Chem Chem Phys*, 2006, **8**, 1371–1377.
6. P. E. Burrows, L. S. Sapochak, D. M. McCarty, S. R. Forrest, and M. E. Thompson, *Appl. Phys. Lett.*, 1994, **64**, 2718–2720.
7. P. Shakya, P. Desai, M. Somerton, G. Gannaway, T. Kreouzis, and W. P. Gillin, *J. Appl. Phys.*, 2008, **103**.

8. V. K. Shukla and S. Kumar, *Opt. Mater.*, 2007, **29**, 1809 – 1816.
9. S. Anderson, M. S. Weaver, and A. J. Hudson, *Synth. Met.*, 2000, **111–112**, 459 – 463.
10. X.-Y. Wang and M. Weck, *Macromolecules*, 2005, **38**, 7219–7224.
11. K. Tanaka and Y. Chujo, *Macromol. Rapid Commun.*, 2012, **33**, 1235–1255.
12. F. Jäkle, *Chem. Rev.*, 2010, **110**, 3985–4022.
13. Y.-L. Rao and S. Wang, *Inorg. Chem.*, 2011, **50**, 12263–12274.
14. A. Nagai and Y. Chujo, *Chem. Lett.*, 2010, **39**, 430–435.
15. F. Jäkle, *Coord. Chem. Rev.*, 2006, **250**, 1107 – 1121.
16. Y. Qin, I. Kiburu, S. Shah, and F. Jäkle, *Org. Lett.*, 2006, **8**, 5227–5230.
17. Y. Nagata and Y. Chujo, *Macromolecules*, 2008, **41**, 2809–2813.
18. Y. Tokoro, A. Nagai, K. Kokado, and Y. Chujo, *Macromolecules*, 2009, **42**, 2988–2993.
19. I. Hernández and W. P. Gillin, *J. Phys. Chem. B*, 2009, **113**, 14079–14086.
20. U. Mitschke and P. Bauerle, *J Mater Chem*, 2000, **10**, 1471–1507.
21. Y. Shirota and H. Kageyama, *Chem. Rev.*, 2007, **107**, 953–1010.
22. S. L. Hellstrom, J. Ugolotti, G. J. P. Britovsek, T. S. Jones, and A. J. P. White, *New J Chem*, 2008, **32**, 1379–1387.
23. L. S. Sapochak, A. Padmaperuma, N. Washton, F. Endrino, G. T. Schmett, J. Marshall, D. Fogarty, P. E. Burrows, and S. R. Forrest, *J. Am. Chem. Soc.*, 2001, **123**, 6300–6307.
24. M. Brinkmann, G. Gadret, M. Muccini, C. Taliani, N. Masciocchi, and A. Sironi, *J. Am. Chem. Soc.*, 2000, **122**, 5147–5157.
25. Y.-K. Lan and C.-I. Huang, *J. Phys. Chem. B*, 2008, **112**, 14857–14862.
26. J.-L. Brédas, D. Beljonne, V. Coropceanu, and J. Cornil, *Chem. Rev.*, 2004, **104**, 4971–5004.
27. G. R. Hutchison, M. A. Ratner, and T. J. Marks, *J. Am. Chem. Soc.*, 2005, **127**, 16866–16881.
28. W.-Q. Deng and W. A. Goddard, *J. Phys. Chem. B*, 2004, **108**, 8614–8621.
29. V. Stehr, R. F. Fink, B. Engels, J. Pflaum, and C. Deibel, *J. Chem. Theory Comput.*, 2014, **10**, 1242–1255.
30. M. Mamada, H. Katagiri, M. Mizukami, K. Honda, T. Minamiki, R. Teraoka, T. Uemura, and S. Tokito, *ACS Appl. Mater. Interfaces*, 2013, **5**, 9670–9677.
31. H. Mori, X. Chen, N. Chang, S. Hamao, Y. Kubozono, K. Nakajima, and Y. Nishihara, *J. Org. Chem.*, **0**, null.
32. B. C. Lin, C. P. Cheng, Z.-Q. You, and C.-P. Hsu, *J. Am. Chem. Soc.*, 2005, **127**, 66–67.
33. C. Liang and M. D. Newton, *J. Phys. Chem.*, 1992, **96**, 2855–2866.
34. R. A. Marcus and N. Sutin, *Biochim. Biophys. Acta BBA - Rev. Bioenerg.*, 1985, **811**, 265 – 322.
35. P. F. Barbara, T. J. Meyer, and M. A. Ratner, *J. Phys. Chem.*, 1996, **100**, 13148–13168.
36. E. Laborda, M. C. Henstridge, C. Batchelor-McAuley, and R. G. Compton, *Chem Soc Rev*, 2013, **42**, 4894–4905.
37. G. Wesela-Bauman, P. Ciećwierz, K. Durka, S. Luliński, J. Serwatowski, and K. Woźniak, *Inorg. Chem.*, 2013, **52**, 10846–10859.
38. L. Merrill and W. A. Bassett, *Rev. Sci. Instrum.*, 1974, **45**, 290–294.
39. S. A. Moggach, D. R. Allan, S. Parsons, and J. E. Warren, *J. Appl. Crystallogr.*, 2008, **41**, 249–251.
40. G. J. Piermarini, S. Block, J. D. Barnett, and R. A. Forman, *J. Appl. Phys.*, 1975, **46**, 2774–2780.
41. Bruker AXS Inc., *SMART*, Bruker–Nonius, Madison, Wisconsin, USA, 2002.
42. Bruker AXS Inc., *SAINT*, Bruker–Nonius, Madison, Wisconsin, USA, 2004.
43. Bruker AXS Inc., *SADABS*, Madison, Wisconsin, USA, 2004.
44. A. Dawson, D. R. Allan, S. Parsons, and M. Ruf, *J. Appl. Crystallogr.*, 2004, **37**, 410–416.
45. L. Palatinus and G. Chapuis, *J. Appl. Crystallogr.*, 2007, **40**, 786–790.

46. P. W. Betteridge, J. R. Carruthers, R. I. Cooper, K. Prout, and D. J. Watkin, *J. Appl. Crystallogr.*, 2003, **36**, 1487.
47. J. R. Carruthers and D. J. Watkin, *Acta Crystallogr. Sect. A*, 1979, **35**, 698–699.
48. H. Fuess (Ed.),, *International Tables for Crystallography,Mathematical, Physical and Chemical Tables*, Chester, 2006, vol. C.
49. A. Gavezzotti, *J. Phys. Chem. B*, 2003, **107**, 2344–2353.
50. A. Gavezzotti, *J. Phys. Chem. B*, 2002, **106**, 4145–4154.
51. A. Gavezzotti, *J. Chem. Theory Comput.*, 2005, **1**, 834–840.
52. A. Gavezzotti, *CrystEngComm*, 2003, **5**, 429–438.
53. L. Maschio, B. Civalleri, P. Ugliengo, and A. Gavezzotti, *J. Phys. Chem. A*, 2011, **115**, 11179–11186.
54. M. J. Frisch, G. W. Trucks, H. B. Schlegel, G. E. Scuseria, M. A. Robb, J. R. Cheeseman, G. Scalmani, V. Barone, B. Mennucci, G. A. Petersson, H. Nakatsuji, M. Caricato, X. Li, H. P. Hratchian, A. F. Izmaylov, J. Bloino, G. Zheng, J. L. Sonnenberg, M. Hada, M. Ehara, K. Toyota, R. Fukuda, J. Hasegawa, M. Ishida, T. Nakajima, Y. Honda, O. Kitao, H. Nakai, T. Vreven, J. A. Montgomery, Jr., J. E. Peralta, F. Ogliaro, M. Bearpark, J. J. Heyd, E. Brothers, K. N. Kudin, V. N. Staroverov, T. Keith, R. Kobayashi, J. Normand, K. Raghavachari, A. Rendell, J. C. Burant, S. S. Iyengar, J. Tomasi, M. Cossi, N. Rega, J. M. Millam, M. Klene, J. E. Knox, J. B. Cross, V. Bakken, C. Adamo, J. Jaramillo, R. Gomperts, R. E. Stratmann, O. Yazyev, A. J. Austin, R. Cammi, C. Pomelli, J. W. Ochterski, R. L. Martin, K. Morokuma, V. G. Zakrzewski, G. A. Voth, P. Salvador, J. J. Dannenberg, S. Dapprich, A. D. Daniels, O. Farkas, J. B. Foresman, J. V. Ortiz, J. Cioslowski, and D. J. Fox, *Gaussian 09*, Gaussian, Inc, Wallingford CT, 2010.
55. A. D. Becke, *Phys Rev A*, 1988, **38**, 3098–3100.
56. C. Lee, W. Yang, and R. G. Parr, *Phys Rev B*, 1988, **37**, 785–789.
57. S. Grimme, *J. Comput. Chem.*, 2006, **27**, 1787–1799.
58. R. Krishnan, J. S. Binkley, R. Seeger, and J. A. Pople, *J. Chem. Phys.*, 1980, **72**, 650–654.
59. P. J. Hay and W. R. Wadt, *J. Chem. Phys.*, 1985, **82**, 270–283.
60. M. N. Glukhovtsev, A. Pross, M. P. McGrath, and L. Radom, *J. Chem. Phys.*, 1995, **103**, 1878–1885.
61. A. L. L. East, G. M. Berner, A. D. Morcom, and L. Mihichuk, *J. Chem. Theory Comput.*, 2008, **4**, 1274–1282.
62. S. S. Hepperle, Q. Li, and A. L. L. East, *J. Phys. Chem. A*, 2005, **109**, 10975–10981.
63. C. Sosa, J. Andzelm, B. C. Elkin, E. Wimmer, K. D. Dobbs, and D. A. Dixon, *J. Phys. Chem.*, 1992, **96**, 6630–6636.
64. N. Godbout, D. R. Salahub, J. Andzelm, and E. Wimmer, *Can. J. Chem.*, 1992, **70**, 560–571.
65. F. H. Allen and I. J. Bruno, *Acta Crystallogr. Sect. B*, 2010, **66**, 380–386.
66. H. Putz and K. Brandenburg, *Diamond - Crystal and Molecular Structure Visualization*, Germany, 2012.
67. W. Humphrey, A. Dalke, and K. Schulten, *J. Mol. Graph.*, 1996, **14**, 33 – 38.
68. T. A. Keith, *AIMAll*, TK Gristmill Software, Overland Park KS, USA, 2012.
69. M. A. Spackman and J. J. McKinnon, *CrystEngComm*, 2002, **4**, 378–392.
70. M. A. Spackman and D. Jayatilaka, *CrystEngComm*, 2009, **11**, 19–32.
71. J. J. McKinnon, M. A. Spackman, and A. S. Mitchell, *Acta Crystallogr. Sect. B*, 2004, **60**, 627–668.
72. J. J. McKinnon, D. Jayatilaka, and M. A. Spackman, *Chem Commun*, 2007, **0**, 3814–3816.
73. R. Berger, G. Resnati, P. Metrangolo, E. Weber, and J. Hulliger, *Chem Soc Rev*, 2011, **40**, 3496–3508.
74. P. A. Wood, J. J. McKinnon, S. Parsons, E. Pidcock, and M. A. Spackman, *CrystEngComm*, 2008, **10**, 368–376.

75. M. O. Sinnokrot and C. D. Sherrill, *J. Phys. Chem. A*, 2006, **110**, 10656–10668.
76. M. I. Aroyo, A. Kirov, C. Capillas, J. M. Perez-Mato, and H. Wondratschek, *Acta Crystallogr. Sect. A*, 2006, **62**, 115–128.
77. Aroyo Mois Ilia, Perez-Mato Juan Manuel, Capillas Cesar, Kroumova Eli, Ivantchev Svetoslav, Madariaga Gotzon, Kirov Asen, and Wondratschek Hans, *Z. Für Krist.*, 2009, **221**, 15.
78. M. I. Aroyo, J. M. Perez-Mato, D. Orobengoa, E. Tasci, G. De La Flor, and A. Kirov, *Bulg. Chem. Commun.*, 2011, **43**, 183–197.
79. C. Slebodnick, J. Zhao, R. Angel, B. E. Hanson, Y. Song, Z. Liu, and R. J. Hemley, *Inorg. Chem.*, 2004, **43**, 5245–5252.
80. N. P. Funnell, A. Dawson, D. Francis, A. R. Lennie, W. G. Marshall, S. A. Moggach, J. E. Warren, and S. Parsons, *CrystEngComm*, 2010, **12**, 2573–2583.
81. M. J. Cliffe and A. L. Goodwin, *J. Appl. Crystallogr.*, 2012, **45**, 1321–1329.